UDC 621.314 https://doi.org/10.20998/2074-272X.2023.5.06

N. Zerzouri, N. Ben Si Ali, N. Benalia

A maximum power point tracking of a photovoltaic system connected to a three-phase grid using a variable step size perturb and observe algorithm

Purpose. *The production of electricity from solar energy is necessary because of the global consumption of this energy. This article's study is based on increased energy extraction by improving maximum power point tracking (MPPT). From different MPPT techniques proposed, the perturb and observe (P&O) technique is developed because of its low implementation cost and ease of implementation.* ***Methods***. *A modified variable step-size P&O MPPT algorithm is investigated which uses fuzzy logic to automatically adjust step-size to better track maximum power point, compared with the conventional fixed step-size method. The variable step P&O improves the speed and the tracking accuracy. This controller is implemented on a boost DC-DC power converter to track the maximum power point. The suggested controlled solar energy system includes a boost converter, a voltage-source inverter, and a grid filter. The control scheme of a three-phase current-controlled pulse-width modulation inverter in rotating synchronous coordinate d-q with the proposed MPPT algorithm and feed-forward compensation is studied.* ***Results***. *The photovoltaic grid-connected system controller employs multi-loop control with the filter inductor current of the inverter in the inner loop to achieve a fast dynamic response and the outer loop to control bus voltage for MPPT, the modeling, and control of three phase grid connected to photovoltaic generator is implemented in the MATLAB/Simulink environment and validated by simulation results.* References 27, tables 5, figures 29.

Key words: **photovoltaic generator, perturb and observe maximum power point tracking, modified perturb and observe maximum power point tracking, fuzzy logic control, boost converter, pulse-width modulation inverter, three phase grid.**

Мета. *Виробництво електроенергії із сонячної енергії необхідне через глобальне споживання цієї енергії. Дослідження цієї статті ґрунтується на збільшенні вилучення енергії за рахунок покращення відстеження точки максимальної потужності (MPPT). З різних запропонованих методів MPPT був розроблений метод збурення та спостереження (P&O) через його низьку вартість реалізації та простоту реалізації.* ***Методи***. *Досліджується модифікований алгоритм P&O MPPT зі змінним розміром кроку, який використовує нечітку логіку для автоматичного налаштування розміру кроку для кращого відстеження точки максимальної потужності порівняно із звичайним методом фіксованого розміру кроку. Змінний крок P&O підвищує швидкість та точність відстеження. Цей контролер реалізований на перетворювачі, що підвищує потужності постійного струму для відстеження точки максимальної потужності. Пропонована керована сонячна енергетична система включає підвищуючий перетворювач, інвертор джерела напруги і мережевий фільтр. Досліджується схема управління трифазним струмокерованим інвертором з широтно-імпульсною модуляцією в синхронній координаті, що обертається, d-q із запропонованим алгоритмом MPPT і попереджувальною компенсацією.* ***Результати***. *Контролер фотоелектричної системи, підключеної до мережі, використовує багатоконтурне керування зі струмом індуктора фільтра інвертора у внутрішньому контурі для досягнення швидкого динамічного відгуку та зовнішнім контуром для керування напругою шини для MPPT, моделювання та керування трифазною мережею. підключений до фотогальванічного генератора, реалізований у середовищі MATLAB/Simulink та підтверджений результатами моделювання.* Бібл. 27, табл. 5, рис. 29.

Ключові слова: **фотоелектричний генератор, збурення та відстеження точки максимальної потужності, модифіковане збурення та відстеження точки максимальної потужності, нечітке логічне управління, підвищуючий перетворювач, інвертор з широтно-імпульсною модуляцією, трифазна мережа.**

Introduction. World energy consumption is mainly covered by fossil fuels (oil, coal, natural gas, and nuclear) which gives rise to greenhouse gas emissions and therefore an increase in pollution. The additional danger is that excessive consumption of the stock of natural resources reduces the reserves of this type of energy dangerously for future generations. In this sense, the world converges toward using renewable energies, which are available and inexhaustible and inhibit emitting CO_2 gas. The development and integration of renewable energies into electrical production and distribution networks pose major technical challenges today. These networks must support a high demand, react quickly and safely to expected and unanticipated variations, and adapt to the constraints of users and environmental constraints. However, the major problem of this electrical energy production technique lies in the design and the realization of the photovoltaic (PV) systems, making it possible to ensure the optimal operation of the PV modules in various conditions. Since PV cells have electrical characteristics (current-voltage) non-linear, which strongly depend on climatic conditions, such as solar radiation and temperature, these climatic variations lead to non-linear and fluctuating power output. For this and with the development of specific power electronics for PV applications, several innovative conversion systems have been designed, particularly inverters with input matching stages that provide maximum power point (MPP) tracking. Indeed, these devices make it possible to adapt and optimize the production of PV through DC-DC power converters inserted between PV modules and inverter input. Usually, this equipment has electrical management mechanisms that allow the maximum power to be extracted from the PV generator output and ensure perfect adaptation between the generator's voltage and inverter input voltage regardless of meteorological conditions. These mechanisms are usually called maximum power point tracking (MPPT). In recent years, many different techniques or algorithms for automatically identifying and producing operations at approximately the MPP have been presented with practical implementations in the literature. These methods vary in complexity, cost, range of effectiveness, hardware implementation, popularity, convergence speed, and other respects. MPPT methods can be classified as incremental conductance [1-5], fractional short-circuit current [2], fractional open-circuit voltage [3], load current voltage maximization, ripple correlation control, hill climbing or perturb and observe (P&O) [4], neural network [6], fuzzy logic control and

other MPPT methods [7, 8]. So far, the P&O method is the most commonly used technique in practice, owing to its ease of implementation in a low-cost controller. It has relatively good MPPT performance compared to the other techniques. Nevertheless, the P&O method fails to track the MPP effectively when radiation and temperature conditions change rapidly.

The conventional P&O is usually implemented with a fixed step size by which the controlled parameter such as reference voltage or duty cycle is adjusted; large step-size values increase the losses in the steady state condition due to large oscillation around the MPP, while small step-size values slow down the tracking speed when the atmospheric conditions quickly change. A trade-off between steady-state accuracy and dynamic tracking should be performed to solve this problem. In the literature, many improvements of the P&O method have been proposed to reduce the oscillation around the MPP in steady-state conditions. However, they increase the complexity, slow the tracking speed when the atmospheric conditions rapidly change and, degrade the algorithm efficiency on cloudy days [9]. To solve this problem, many authors have used P&O MPPT with variable step sizes, each in her own way and they deduced results that prove an improvement in tracking of maximum power. We find in the reference [8] many MPPT methods are reviewed and have been made to improve the conventional MPPT methods. However, in [10–12] shows the performance with the modified P&O algorithm which gives a faster response than the traditional P&O algorithm under variable irradiance conditions during peak power generation the impacts of partial shading conditions and temperature led to a high convergence rate with less overshoot and oscillation. On the other hand, [11] proposes a modified hill-climbing algorithm the proposed algorithm has good steady-state and dynamic performances. In work [13] introduced MPPT with a P&O algorithm with variable step size based on modified shuffled frog leaping algorithm (MSFLA) and sliding mode control (SMC) for PV power systems. The operation of the system with various partial shading regimes was evaluated and it was demonstrated that the developed MSFLA-SMC combinatorial scheme gives good efficiency in output power with significantly better response time and dynamic behavior.

In this study, P&O MPPT with variable step size is proposed. The step size is automatically tuned according to the variation of the atmospheric conditions, using a fuzzy logic controller.

To control active and reactive power for grid-connected inverters, the most common method has been used voltage-oriented control (VOC) which depends on two cascaded loops. The outer loop or voltage loop is tied to the DC link capacitor voltage, where a PI controller is used to generate the reference current for the inner or current loop. Then, two PI controllers are used to control the currents, and hence active/reactive power control.

The goal of the paper is the extraction of the maximum powers provided by the photovoltaic generator using the perturb and observe algorithm with fixed step size and variable step size adjusted by a fuzzy logic controller, another objective is the control of this power to be injected into a three-phase distribution network via a two-stage conversion system. The schematic of the proposed system is shown in Fig. 1, which illustrates the three-phase grid-connected PV generation system. The proposed system consists of two main parts; the first part is a power scheme, which includes: a PV array supply, DC link capacitor, boost converter, three-phase inverter, RL filter, and the three-phase utility grid. The second is the control scheme MPPT by using different MPPT techniques and the inverter controller with a three-phase PV grid-connected system.

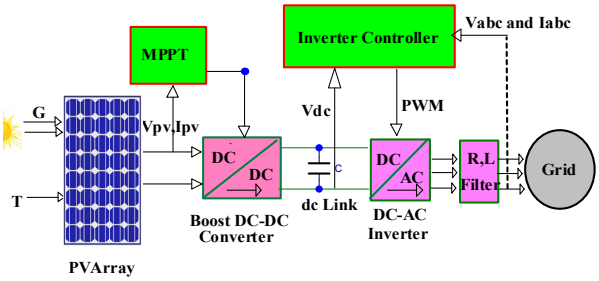

Fig. 1. Configuration of the proposed two-stage grid-connected PV system

PV cell model. Figure 2 shows the PV model based on a one-diode equivalent circuit. In the literature, an ideal *p-n* junction PV cell is often modeled as an electric current generator whose behavior is equivalent to an ideal current source which models the photoelectric current (I_{ph}) associated with a parallel diode which models the *p-n* junction. To take into account all the dissipative phenomena present during the conversion of light energy at the level of the cell, the circuit is completed by two resistors, one in series (R_s) and the other in parallel (R_{sh}). The series resistance characterizes the losses by the Joule effect and the parallel resistance characterizes the leakage current at the level of the *p-n* junction.

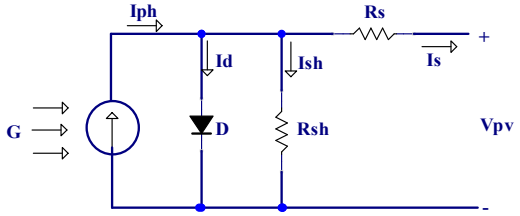

Fig. 2. The equivalent circuit of a solar cell

The PV cell output current I_{PV} (Fig. 2) is given as [14, 15]:

$$I = I_{ph} - I_s\left(\exp\left[\frac{q}{A\cdot K\cdot T_c}\cdot\left(V_{pv}+I_{pv}R_s\right)-1\right]\right) - \left(\frac{V_{pv}+I_{pv}R_s}{R_{sh}}\right), \quad (1)$$

where V_{pv} is the PV array output voltage; I_{pv} is the PV array output current; I_{ph} is the PV cell photocurrent; I_s is the PV cell saturation current; q is the electron charge (q = 1.602·10^{-19} C); A is the *p-n* junction ideality factor; K is the Boltzmann constant (K = 1.38·10^{-23} J/K); T_c is the absolute working temperature.

The photocurrent I_{ph} is related to the cell's operating temperature and solar intensity as:

$$I_{ph} = \left[I_{sc} + K_i\left(T_c - T_{ref}\right)\right]\frac{G}{1000}, \quad (2)$$

where I_{sc} is the short circuit current at standard temperature and irradiance condition (G = 1000 W/m^2 and T_{ref} = 25 °C); K_i is the short circuit current temperature coefficient; T_{ref} is the PV cell reference temperature.

PV cell reverse saturation current I_{rs} varies with the cell temperature [16, 17] as:

$$I_{rs} = \frac{I_{sc} + K_i\left(T_c - T_{ref}\right)}{\exp\left(\frac{V_{oc} + K_i\left(T_c - T_{ref}\right)}{V_t}\right) - 1}; \quad (3)$$

$$V_t = \frac{N_s \cdot K \cdot T_c}{q}, \quad (4)$$

where V_{oc} is the open-circuit voltage at reference temperature T_{ref}; V_t is the junction thermal voltage; N_s is the number of solar cells connected in series (N_s = 1 for the solar cell).

The PV cell saturation current I_s varies with temperature [18] as:

$$I_s = I_{rs}\left(\frac{T_c}{T_{ref}}\right)^3 \exp\left[\frac{q \cdot E_g}{A \cdot K}\left(\frac{1}{T_{ref}} - \frac{1}{T_c}\right)\right], \quad (5)$$

where E_g is the band energy of the semiconductor used in the cell.

In this work, the studied PV field is composed of two PV arrays, each comprising 2 series and 9 parallel connected modules of type Canadian Solar CS6X-305P. Each module contains a series of 72 polycrystalline silicon cells; resulting in total peak power of 305 W. Table 1 shows the specifications of the used PV modules in standard conditions.

Table 1

Parameters of Canadian Solar CS6X-305P PV module

Parameters	Value
Peak power, W	305.285
Peak power voltage, V	36.3
Peak power current, A	8.41
Short-circuit current, A	8.97
Open circuit voltage, V	44.8

The characteristics (I-V) and (P-V) of the studied PV field, under standard conditions of solar irradiation and temperature, is given in Fig. 3.

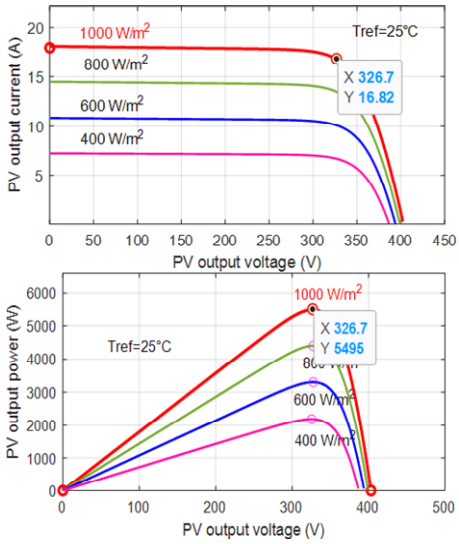

Fig. 3. (I-V) and (P-V) characteristic curves of a solar module at 25 °C temperature and 1000 W/m^2 irradiance level

Boost converter model. DC-DC converters have wide applications in PV systems. Whether it is a boost converter [15-19], buck-boost converter [20, 21], or buck converter [13]. DC-DC converters are considered the main element in the MPPT process; without them, the maximum power could not be achieved. In this study boost converter is used to change the terminal voltage of the PV array and from which MPPT can be obtained. The boost converter presented in Fig. 4 is composed of an inductance L_{pv}, a diode D, capacitors C_{pv}, C_{dc} and a switch S. The converter has two modes (states) of operation based on the switch action OFF and ON. The mathematic expression of the voltage and current on the input and output side of the DC-DC boost converter at duty cycle (D) can be described as:

$$V_{dc} = \frac{V_{pv}}{1 - D}; \quad (6)$$

$$I_{dc} = I_{pv}\left(1 - D\right). \quad (7)$$

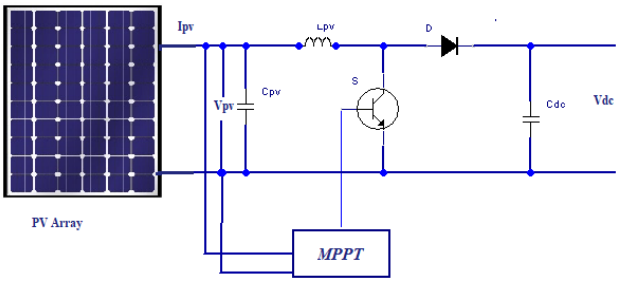

Fig. 4 Step-up boost converter

In the current source PV cell, the capacitor C_{pv} is evaluated by (8) and the standards of its elements:

$$C_{pv} = \frac{D \cdot V_{pv}}{4 \cdot \Delta V_{pv} \cdot f_s^2 \cdot L_{pv}}; \quad (8)$$

$$D = 1 - \frac{V_{pv}}{V_{dc}}; \quad (9)$$

$$L_{pv} = \frac{V_{pv} \cdot \left(V_{dc} - V_{pv}\right)}{\Delta I_{L_{pv}} \cdot f_s \cdot V_{dc}}; \quad (10)$$

$$\Delta I_{L_{pv}} = 0.13 \cdot I_{pv} \cdot \frac{V_{dc}}{V_{pv}}; \quad (11)$$

$$C_{dc} \geq \frac{P_{pv}}{\Delta V_o \cdot f_s \cdot V_{dc}}, \quad (12)$$

where V_{pv} is the converter input voltage; I_{pv} is the array maximum current; P_{PV} is the nominal power of PV; f_s is the converting frequency; C_{pv} is the link capacitance of PV; C_{dc} is the capacitance of DC-link; L_{pv} is the inductance of boost converter; V_{dc} is the boost converter output voltage; ΔV_{pv} is the voltage variation; ΔI_{Lpv} is the current ripple of boost inductance; ΔV_o is the ripple of output voltage.

Modeling and control of DC/AC inverter. The main inverter function is to interface the PV generator with the network (Fig. 5). At the same time, the inverter is used to transform the DC voltage on the output side of the boost converter (the intermediate circuit of the inverter) into an AC voltage at its output. Voltage-source converter (VSC) is controlled in the rotating d-q frame to inject a

controllable three-phase alternating current into the network. Current is injected in phase with the grid voltage to achieve unity power factor operation. The three-phase VSC is made up of three arms of two switches each reversible in current, they are made by controllable semiconductors on opening and closing (of the IGBT type in almost all cases). A recovery diode is mounted head to tail with the controllable semiconductor for each switch. A filter is placed between the network and the inverter, connecting them to the common point of interconnection.

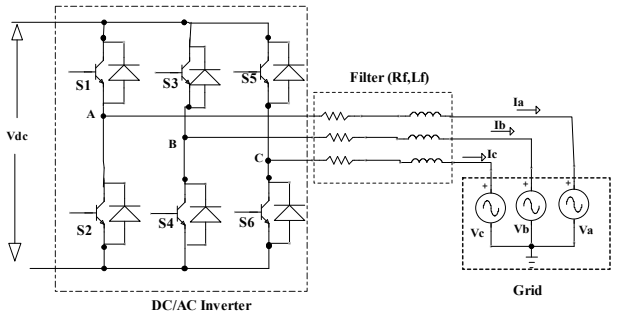

Fig. 5. Three-phase grid-connected inverter

The three-phase equations of the electrical network can be established as [22, 23]:

$$\begin{cases} u_a = R_f \cdot i_a + L_f \cdot \dfrac{\mathrm{d}i_a}{\mathrm{d}t} + v_a; \\ u_b = R_f \cdot i_b + L_f \cdot \dfrac{\mathrm{d}i_b}{\mathrm{d}t} + v_b; \\ u_c = R_f \cdot i_c + L_f \cdot \dfrac{\mathrm{d}i_c}{\mathrm{d}t} + v_c; \end{cases} \quad (13)$$

where v_a, v_b, v_c are the grid voltages; i_a, i_b, i_c are the injected currents; u_a, u_b, u_c are the inverter side voltages.

This type of inverter is known as an on two levels because its output voltage has two voltage levels ($+V_{dc}$ and $-V_{dc}$). Using the a-b-c to d-q transformations, the converter 3-phase currents and voltages are expressed in a 2-axis d-q reference frame, synchronously rotating at a given AC frequency ω:

$$\begin{cases} u_d = R_f \cdot i_d + L_f \cdot \dfrac{\mathrm{d}i_d}{\mathrm{d}t} - \omega \cdot L_f \cdot i_q + v_d; \\ u_q = R_f \cdot i_q + L_f \cdot \dfrac{\mathrm{d}i_q}{\mathrm{d}t} - \omega \cdot L_f \cdot i_d + v_q. \end{cases} \quad (14)$$

The current controller and control equations of u_d and u_q can be rewritten as:

$$\begin{cases} u_d = P \cdot I \cdot \left(I_{dref} - I_d\right) - \omega \cdot L_f \cdot i_q + v_d; \\ u_q = P \cdot I \cdot \left(I_{qref} - Iq\right) + \omega \cdot L_f \cdot i_d + v_q. \end{cases} \quad (15)$$

The active and reactive power injected by the PV generator in the grid can be defined for a balanced three-phase system as follows [17]:

$$P = \frac{3}{2} \cdot \left(v_d \cdot i_d + v_q \cdot i_q\right); \quad Q = \frac{3}{2} \cdot \left(v_q \cdot i_d + v_d \cdot i_q\right). \quad (16)$$

Applying the voltage orientation technique to the d-axis, the active and reactive power (16) can be rewritten as:

$$P = \frac{3}{2} \cdot v_d \cdot i_d; \quad Q = -\frac{3}{2} \cdot v_d \cdot i_q. \quad (17)$$

According to (17), the active power can be controlled by the current i_d, and the reactive power can be controlled by the current i_q.

DC-link voltage control. The DC voltage controller is discussed as the outer controller. Dimensioning of the DC link voltage controller is determined by the function between the current reference value to be given and the DC link voltage [24]. The general model of the external controller can thus be given in Fig. 6. For the PI controller block of the function of $K(s)$, the outer voltage control can be implemented as:

$$i_{dref} = \left(U_{dcref} - U_{dc}\right) \cdot \left(K_{pu} + \frac{K_{iu}}{s}\right). \quad (18)$$

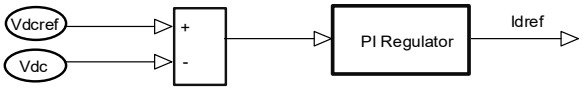

Fig. 6. Model of the DC-voltage controller

The phase-locked loop (PLL) technique [25] has been used to synthesize the electrical system's phase and frequency information, especially when interfacing with power electronic devices. PLL block [26] measures the system frequency and provides the phase synchronous angle θ (more precisely [sinθ, cosθ]) for the d-q transformations block. In the steady state, sinθ is in phase with the fundamental (positive sequence) of α component and phase A. In the three-phase system, the d-q transform of the three-phase variables has the same characteristics and the PLL system can be implemented using the d-q transform. The block diagram of the PLL system is described in Fig. 7.

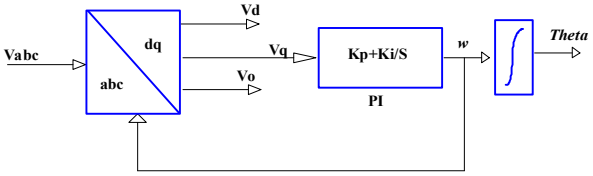

Fig. 7. Schematic diagram of the PLL

Fixed step size P&O algorithm. The P&O method compares the power of the previous step with the new step's power to increase or decrease the tension in search of the MPP. According to [6–10, 13–26], the MPP value is never definitively reached since the disturbances only leave the system oscillating close to the MPP in a steady state. The P&O method presents good results when the irradiance or temperature does not change rapidly with time. On the other hand, among the disadvantages of the method, in addition to the error in steady state, the dynamic response is considered slow when there are rapid temperature and solar radiation changes. The flowchart of this technique with the reference voltage variation is shown in Fig. 8.

Generally, the P&O MPPT algorithm run with a fixed step size. The P&O MPPT with fixed step size gives a good dynamic performance, he converges faster to a steady state but the oscillation is much higher. So, this hurts the MPPT efficiency. A solution that remedies this problem is the variable-step P&O algorithm which has been developed [11, 12]. The proposed MPPT algorithm is based on the conventional P&O algorithm; a fuzzy logic controller block is used to provide variable step size to overcome the limitation that exists in conventional P&O algorithm implementations. The flow chart of the proposed P&O algorithm with variable step size is illustrated in Fig. 9.

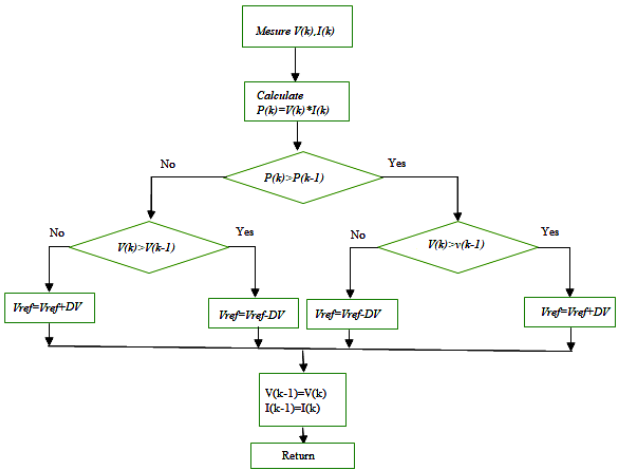

Fig. 8. Flowchart for MPPT for P&O algorithm

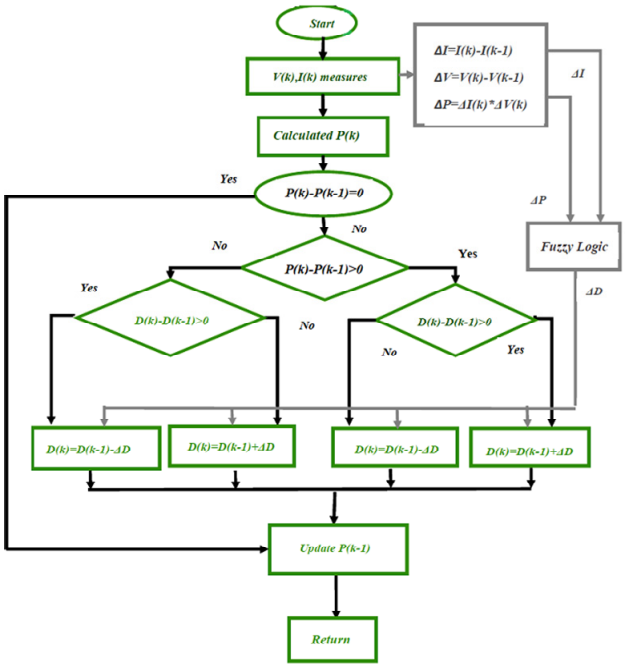

Fig .9. Block diagram of the proposed P&O with a variable step size

When the operating point is far from the MPP, the fuzzy logic control (FLC) adjusts the step size to a large value, and if the operating point is close to the MPP, the step size value is set to a small value.

FLC used as the variable step size. Control by FLC is a method that allows the construction of non-linear controllers from heuristic information from the specialist's knowledge FLC consists of the variation of voltage (or current) and power of the PV array, and according to these variations, the algorithm acts on the converter, through a pulse-width modulation, to correct the MPP voltage. Fuzzy MPPT is a well-established technique, generally acting on power variation (ΔP) and voltage variation (ΔV). In this work, the variable ΔV was replaced by the current variation (ΔI), because in this implemented arrangement the output variable of the FLC is the variation of the step-size ΔD, which is sent to the P&O algorithm. The input variables, ΔP_{pv} and ΔI_{pv}, of the proposed fuzzy logic variable step-size can be calculated by the following equations, where $P_{pv}(k)$ and $I_{pv}(k)$ are the PV array power and current respectively and $V_{pv}(k)$ is the PV array voltage:

$$\Delta V_{pv} = V_{pv}(k) - V_{pv}(k-1); \tag{19}$$

$$\Delta I_{pv} = I_{pv}(k) - I_{pv}(k-1); \tag{20}$$

$$\Delta P_{pv} = \Delta V_{pv} \cdot \Delta I_{pv}. \tag{21}$$

The MPPT fuzzy implemented consisted of input variables ΔP and ΔI, and output variable ΔD. The membership function of the input and the output variables used in this model has the same shape and is shown in Fig. 10–12. All the membership functions are expressed with a triangular function and they consist of 5 fuzzy subsets, which are denoted by NB (negative big), NS (negative small), ZZ (zero), PS (positive, small), and PB (positive big) curves.

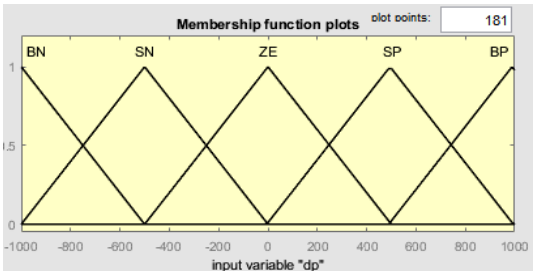

Fig. 10. Input variable ΔP

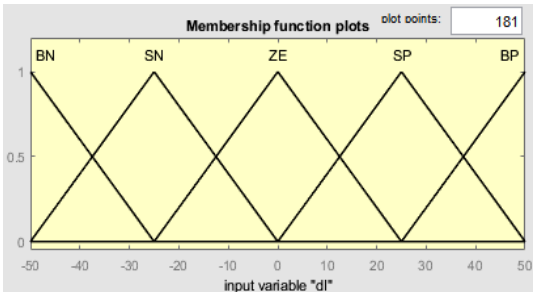

Fig. 11. Input variable ΔI

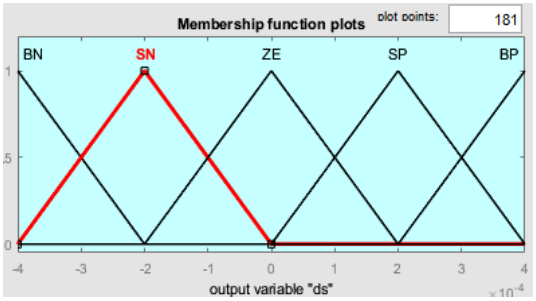

Fig. 12. Output variable ΔD

The fuzzy rule base is a collection of if-then rules which all the information is available for the controlled parameters. Since the number of membership function of each input is 5, then the fuzzy inference rules of the FLC consist of 25 rules as illustrated in Table 2. These rules are used to determine the output of the controller (the variable step-size for the P&O algorithm) to track the MPP and stop iterating once this point is reached.

Table 2

Membership function rules

ΔI_{pv}	ΔP_{pv}				
	NB	NS	ZZ	PS	PB
NB	NB	NS	NS	ZZ	ZZ
NS	NS	ZZ	ZZ	ZZ	PS
ZZ	ZZ	ZZ	ZZ	PS	PS
PS	ZZ	PS	PS	PS	PB
PB	PS	PS	PB	PB	PB

Mamdani's method is used as a fuzzy interface method with max-min operation combined with fuzzy law in this work. After the rules have been evaluated, the output of the fuzzy controller is still a fuzzy set. However, the actual system usually requires a non-fuzzy value of a control. Hence the process of defuzzification is required to as the last step to calculate the crisp output of the proposed fuzzy control. The output of the proposed FLC is defuzzified using the center of gravity method to calculate ΔD computed as:

$$\Delta D(k) = \frac{\sum_{i=1}^{25} \mu(\Delta D_i(k)) \Delta D_i(k)}{\sum_{i=1}^{25} \mu(\Delta D_i(k))}, \quad (22)$$

where ΔD_i is the center of max–min technique composition at the output membership function. The FLC output that is a variable step size $\Delta D(k)$ is used to compute the final duty cycle $D(k)$ as:

$$D(k) = D(k-1) + \Delta D(k). \quad (23)$$

Results and discussion. In this section, the performances of the proposed system are analyzed by simulation in the MATLAB/SimPowerSys environment. Figure 13 shows the architecture of the three-phase two-stage grid-connected PV system, in which the control of injected current, DC link voltage, and MPPT is realized. Also, the influence of variation in climatic conditions on the output performance of the system is realized. After that, a simulation of the P&O and variable step-size P&O (VSP&O) MPPT algorithm with analysis covering stability, time response, oscillation, and overshoot is performed. The simulation parameters of the system are shown in Table 3.

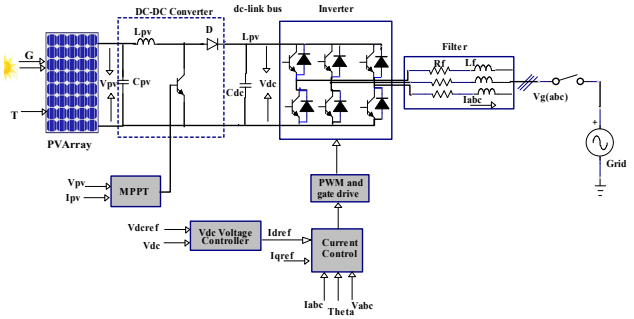

Fig. 13. Model of the three-phase two-stage grid-connected PV system

Table 3

Simulation parameters of the system

Parameters	Value
Input capacitor C_{pv}, F	$5 \cdot 10^{-6}$
Inductance L, H	$3 \cdot 10^{-2}$
DC link capacitor C_{dc}, F	$12 \cdot 10^{-3}$
Switching frequency f_{sw}, kHz	4
DC link voltage V_{dc}, V	700
Grid frequency f, Hz	50
Utility grid voltage V_g, V	220
Inductance filter L_f, H	$5 \cdot 10^{-3}$
Resistance filter R_f, Ω	0.1

The simulation was performed for variable irradiance, with a fixed ambient temperature (25 °C), to test the performance of the two proposed algorithms. The applied irradiance was with a range between 400 and 1000 W/m², at the time step was 0.5 s. The results shown in Fig. 14, 21 are limited to those for the PV array respectively show the irradiance profile applied to the PV array and the output power of the PV array with a comparison between P&O MPPT and VSP&O MPPT which clearly shows the stabilization of the power around its maximum for all the variations of the irradiation in the VSP&O, whereas it oscillates around the maximum power and moves away from the maximum for the weak irradiance in the P&O. In Fig. 15 we observe how the increase in incident solar radiation causes an increase in the current generated, at a constant temperature of 25 °C thus increasing the power produced by the photovoltaic generator as seen in Fig. 16. It is clear that the direct component of the current represented in Fig. 23, coincides perfectly with the reference direct component and that the overshoot with VSP&O is less than in the case of P&O.

Table 4 provides a summary of tracking performance for the VSP&O MPPT and P&O MPPT methods with different levels of illumination.

Table 4

Tracking performance comparison between P&O MPPT and VSP&O MPPT methods

Irradiance / MPPT	G, W/m^2	1000	800	600	400
	P_{max}, W	5495	4402	3302	2189
Irradiance P&O with fixed step-size	P_{pv}, W	5413	4185	3178	2033
	Efficiency η, %	98.5	95.07	96.03	92.86
	Tracking time, s	0.153	0.101	0.046	0.0786
	Steady-state power oscillation	high	V-high	V-high	high
P&O with variable step-size	P_{pv}, W	5438	4365	3272	2175
	Efficiency η, %	98.95	99.04	99.1	99.34
	Tracking time, s	0.149	0.0479	0.0556	0.0151
	Steady-state power oscillation	none	none	none	none

From Fig. 17, 18 of PV current and voltage, it is clear that large oscillations appear around the maximum values when the irradiation is reduced, and they move away from the maximum point when the irradiation becomes very low, these problems disappear when using the VSP&O method, as shown in Fig. 19, 20, where the PV output voltage and current reach the maximum with a rapid time and almost without oscillations. For the three-phase grid-connected system, the phase current and voltage are shown in Fig. 24 which is obtained with a conventional PI controller for both algorithms, to indicate the impact of irradiation variation on the current and the voltage, we focus on the time range [0 – 0.04] s where the irradiation is at 1000 W/m^2. Only the peaks of the current for VSP&O are observed to be reduced concerning P&O and the currents decrease when the irradiation decreases while the amplitude of the voltage remains constant. From Fig. 27 it can be observed that the recorded overshoot of the DC bus voltage is 140 V with P&O, while with VSPO the overshoot is 110 V. From these parameters, the VSP&O performs very well in terms of stability.

To illustrate the impact of the MPPT method on the power quality, a spectral analysis of the current obtained with standard test conditions is performed and the spectrum of the harmonic is shown in Fig. 28, 29. We note that the total harmonic distortion (THD) obtained with P&O is 8.42 % while a THD of 6.17 % was obtained with VSP&O, which proves the effectiveness of the VSP&O algorithm compared to P&O.

It is noticed in the interval [0 – 0.06] s that the transient responses for VSP&O of the active and reactive powers are characterized by a very small overshoot compared to the P&O MPPT, while the steady-state error is close to zero as shown in Fig. 25, 26. According to the results obtained, the VOC strategy with classic PI in terms of speed, system stability, and precision has led to satisfactory results.

From the simulation results, the proposed VSP&O MPPT performs well compared to P&O MPPT.

Comparison with existing variable step size MPPT methods. Table 5 summarizes and compares the performances for each controller, the tracking error and the tracking efficiency reveal at any point the proposed controller is efficient and accurate with regards to harvesting the maximum power from the PV system. Also, Fig. 22 presents the average tracking efficiency of the conventional and proposed techniques [27]:

$$Eff = P_{pv} \cdot 100\% / P_{MPP}. \quad (23)$$

The error is calculated as:

$$Err = (P_{MPP} - P_{pv}) \cdot 100\% / P_{MPP}, \quad (24)$$

where P_{pv} is the power generated by the controller; P_{MPP} is the PV MPP.

Table 5

Comparison between the conventional and VSP&O MPPT technique at 1000 W/m^2 and 25 °C

MPPT Algorithm	Settling time, s	Theoretical power P_{MPP}, W	Output power P_{pv}, W	Efficiency, %	Error, %
Fixed step P&O	0.078	5495	5413	93.04	6.95
Variable step P&O [24]	0.025	13183.3	12576.8	95.4	4.6
Variable step P&O [27]	0.0399	2563	2554	99.6	–
Variable step P&O proposed	0.068	5495	5438	98.95	1.02

Comparing our results with the two references [24] and [27], we notice that the proposed P&O method has also contributed to improving efficiency and reducing oscillations around the MPP.

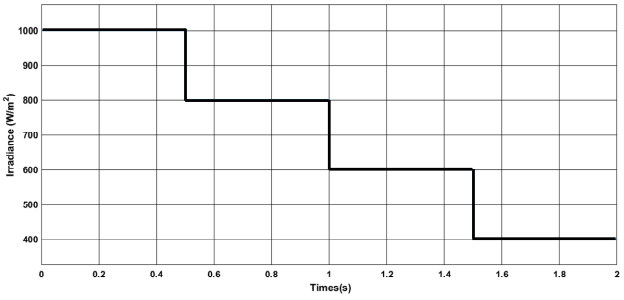

Fig. 14. Irradiance profile

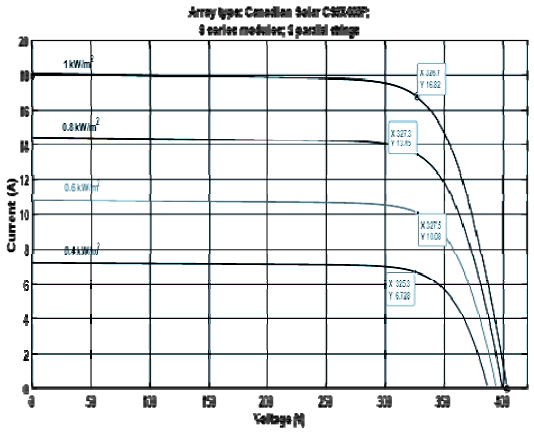

Fig. 15. PV current characteristics under fixed temperature and variable irradiance

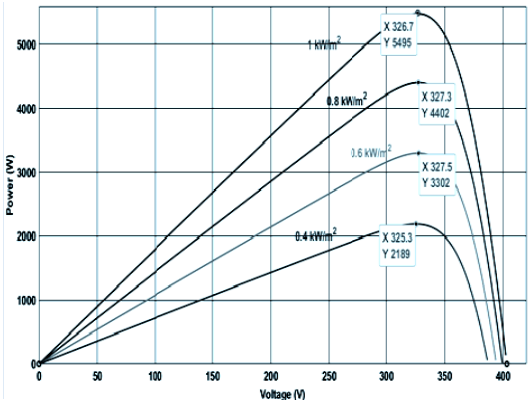

Fig. 16. PV power characteristics under fixed temperature and variable irradiance

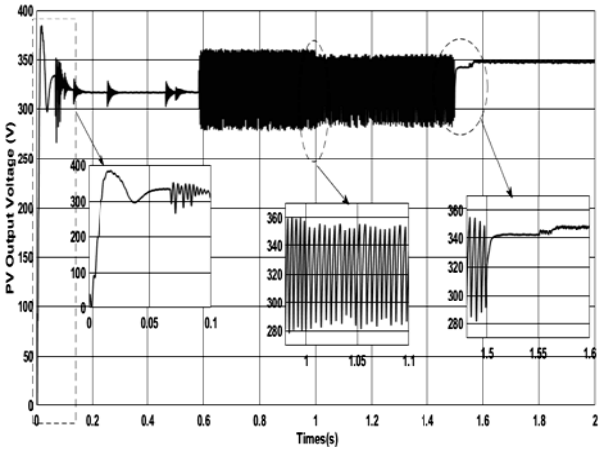

Fig. 17. PV output voltage with fixed step size P&O MPPT

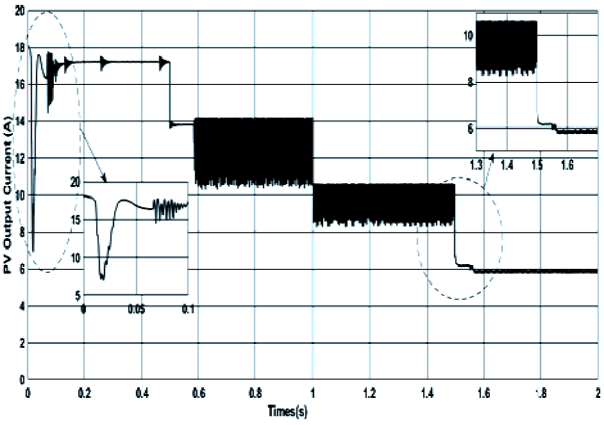

Fig. 18. PV output current with fixed step size P&O MPPT

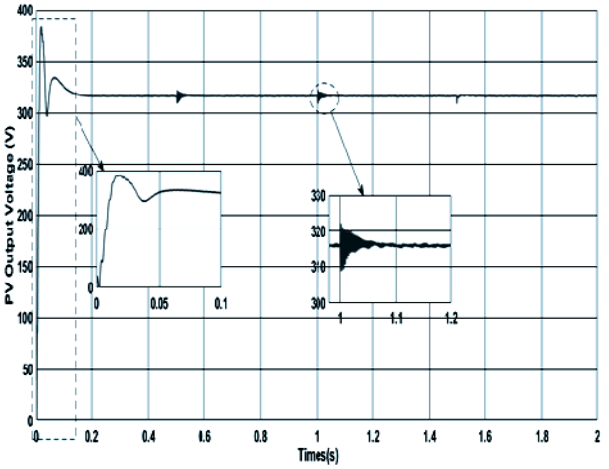

Fig. 19. PV output voltage with variable step size P&O MPPT

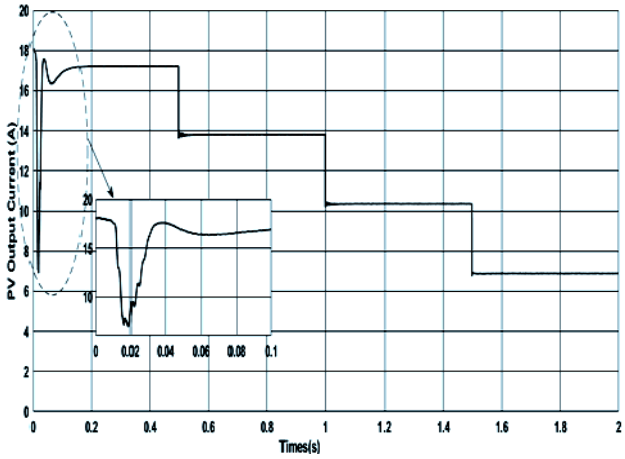

Fig. 20. PV output current with variable step size P&O MPPT

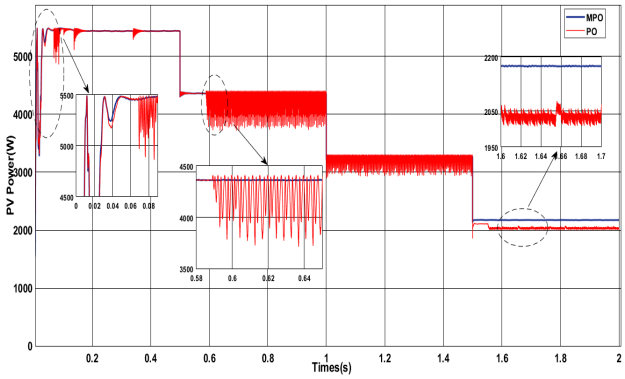

Fig. 21. Simulation result with comparison of fixed step size P&O MPPT and the proposed FLC-based variable step size P&O MPPT with change in irradiance: PV power

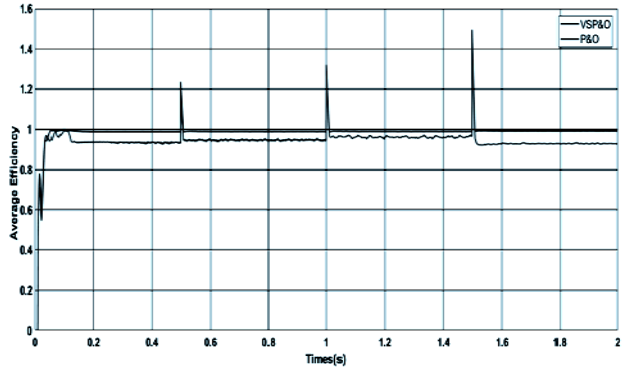

Fig. 22. Efficiency curves

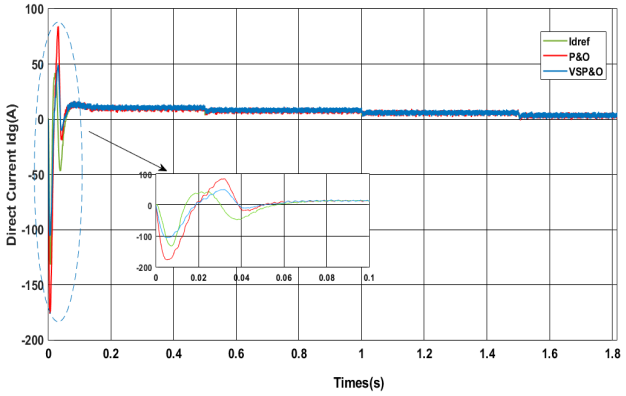

Fig. 23. Simulation result with comparison of fixed step size P&O MPPT and the proposed FLC-based variable step size P&O MPPT with change in irradiance: direct current grid

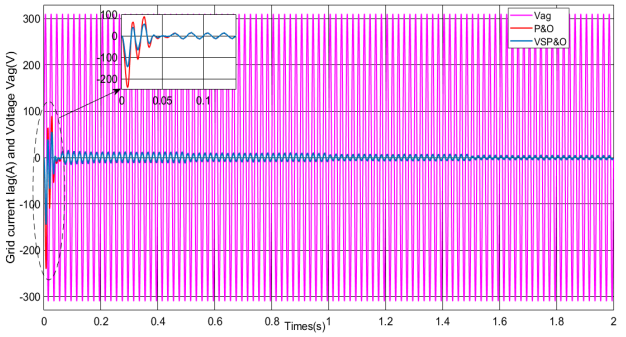

Fig. 24. Simulation result with comparison of fixed step size P&O MPPT and the proposed FLC-based variable step size P&O MPPT with change in irradiance: voltage and current grid

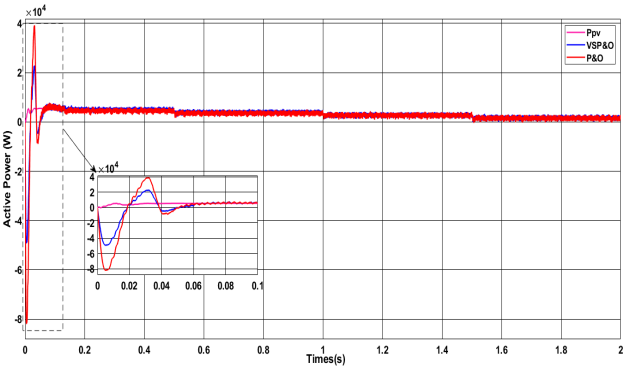

Fig. 25. Simulation result with comparison of fixed step size P&O MPPT and the proposed FLC-based variable step size P&O MPPT with change in irradiance: active power to grid

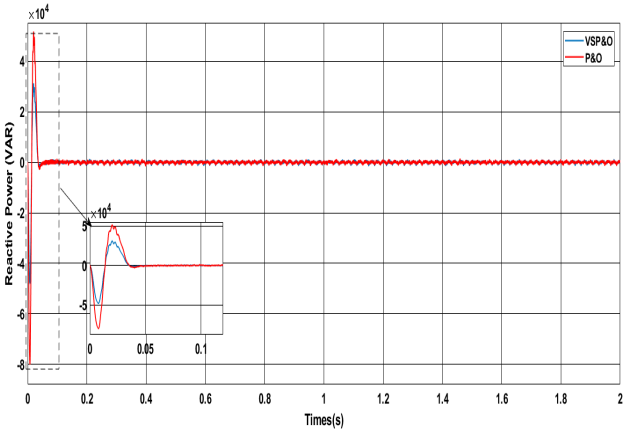

Fig. 26. Simulation result with comparison of fixed step size P&O MPPT and the proposed FLC-based variable step size P&O MPPT with change in irradiance: reactive power to grid

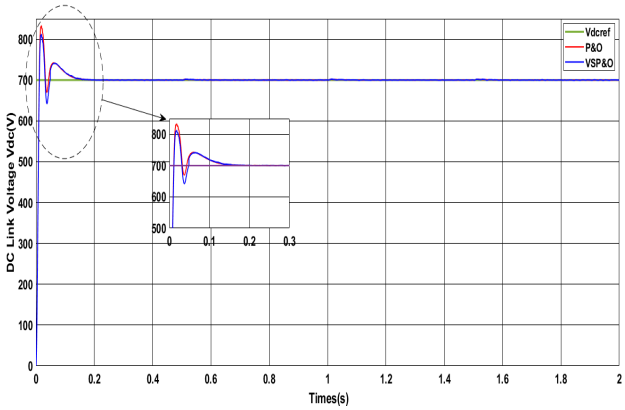

Fig. 27. Simulation result with comparison of fixed step size P&O MPPT and the proposed FLC-based variable step size P&O MPPT with change in irradiance: DC link voltage

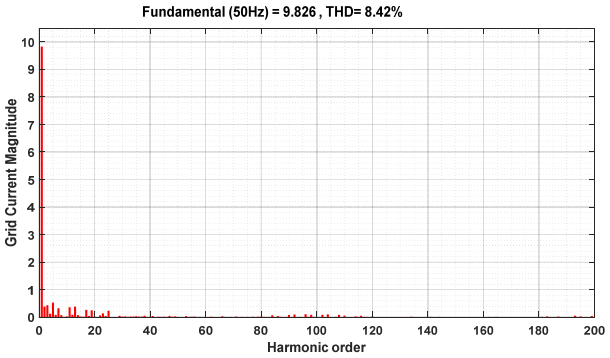

Fig. 28. THD of grid current with P&O MPPT

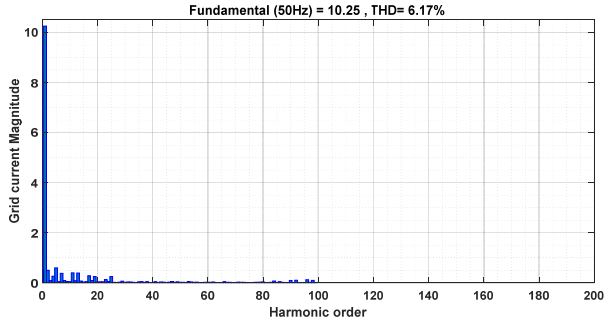

Fig. 29. THD of grid current with VSP&O MPPT

Conclusions. This work presented two photovoltaic generator power maximization algorithms applied to a two-stage three-phase network. A boost converter is used to increase the voltage at the output of the photovoltaic generator by using the two cases of maximum power point tracking, i.e. the perturb and observe method with fixed step and the variable step method calculated by a fuzzy logic block in such a way efficient and precise. The maximum power point tracking variable step size perturb and observe method was found to be more robust compared to the fixed step size perturb and observe method, due to an oscillation-free photovoltaic power response at the instant of irradiance variations. In a steady state, the performance of the maximum power point tracking fixed step size was inferior to the maximum power point tracking variable step size perturb and observe, as it had a larger error, due to the relevance curves and the level of oscillation, especially at the low irradiation.

Conflict of interest. The authors declare that they have no conflicts of interest.

REFERENCES

1. Hlaili M., Mechergui H. Comparison of Different MPPT Algorithms with a Proposed One Using a Power Estimator for Grid Connected PV Systems. *International Journal of Photoenergy*, 2016, pp. 1–10. doi: https://doi.org/10.1155/2016/1728398.

2. Nzoundja Fapi C.B., Wira P., Kamta M., Badji A., Tchakounte H. Real-Time Experimental Assessment of Hill Climbing MPPT Algorithm Enhanced by Estimating a Duty Cycle for PV System. *International Journal of Renewable Energy Research*, 2019, vol. 9, no. 3, pp. 1180-1189. doi: https://doi.org/10.20508/ijrer.v9i3.9432.g7705.

3. Shebani M.M., Iqbal T., Quaicoe J.E. Comparing bisection numerical algorithm with fractional short circuit current and open circuit voltage methods for MPPT photovoltaic systems. *2016 IEEE Electrical Power and Energy Conference (EPEC)*, 2016, pp. 1-5. doi: https://doi.org/10.1109/EPEC.2016.7771689.

4. Louarem S., Kebbab F.Z., Salhi H., Nouri H. A comparative study of maximum power point tracking techniques for a photovoltaic grid-connected system. *Electrical Engineering & Electromechanics*, 2022, no. 4, pp. 27-33. doi: https://doi.org/10.20998/2074-272X.2022.4.04.

5. Shang L., Guo H., Zhu W. An improved MPPT control strategy based on incremental conductance algorithm. *Protection and Control of Modern Power Systems*, 2020, vol. 5, no. 1, p. 14. doi: https://doi.org/10.1186/s41601-020-00161-z.

6. Elhor A., Soares O. Grid-connected PV System with a modified-Neural Network Control. *International Journal of Renewable Energy Research*, 2022, vol. 12, no. 2, pp. 1013-1022. doi: https://doi.org/10.20508/ijrer.v12i2.12754.g8485.

7. Xu S., Shao R., Cao B., Chang L. Single-phase grid-connected PV system with golden section search-based MPPT algorithm. *Chinese Journal of Electrical Engineering*, 2021, vol. 7, no. 4, pp. 25-36. doi: https://doi.org/10.23919/CJEE.2021.000035.

8. Li X., Wang Q., Wen H., Xiao W. Comprehensive Studies on Operational Principles for Maximum Power Point Tracking in Photovoltaic Systems. *IEEE Access*, 2019, vol. 7, pp. 121407-121420. doi: https://doi.org/10.1109/ACCESS.2019.2937100.

9. Manoharan P., Subramaniam U., Babu T.S., Padmanaban S., Holm-Nielsen J.B., Mitolo M., Ravichandran S. Improved Perturb and Observation Maximum Power Point Tracking Technique for Solar Photovoltaic Power Generation Systems. *IEEE Systems Journal*, 2021, vol. 15, no. 2, pp. 3024-3035. doi: https://doi.org/10.1109/JSYST.2020.3003255.

10. Kumar V., Singh M. Derated Mode of Power Generation in PV System Using Modified Perturb and Observe MPPT Algorithm. *Journal of Modern Power Systems and Clean Energy*, 2021, vol. 9, no. 5, pp. 1183-1192. doi: https://doi.org/10.35833/MPCE.2019.000258.

11. Zhu W., Shang L., Li P., Guo H. Modified hill climbing MPPT algorithm with reduced steady-state oscillation and improved tracking efficiency. *The Journal of Engineering*, 2018, vol. 2018, no. 17, pp. 1878-1883. doi: https://doi.org/10.1049/joe.2018.8337.

12. Ali Z.M., Vu Quynh N., Dadfar S., Nakamura H. Variable step size perturb and observe MPPT controller by applying θ-modified krill herd algorithm-sliding mode controller under partially shaded conditions. *Journal of Cleaner Production*, 2020, vol. 271, art. no. 122243. doi: https://doi.org/10.1016/j.jclepro.2020.122243.

13. Mohammadinodoushan M., Abbassi R., Jerbi H., Waly Ahmed F., Abdalqadir kh ahmed H., Rezvani A. A new MPPT design using variable step size perturb and observe method for PV system under partially shaded conditions by modified shuffled frog leaping algorithm- SMC controller. *Sustainable Energy Technologies and Assessments*, 2021, vol. 45, art. no. 101056. doi: https://doi.org/10.1016/j.seta.2021.101056.

14. Kumar N., Saha T.K., Dey J. Multilevel Inverter (MLI)-Based Stand-Alone Photovoltaic System: Modeling, Analysis, and Control. *IEEE Systems Journal*, 2020, vol. 14, no. 1, pp. 909-915. doi: https://doi.org/10.1109/JSYST.2019.2900485.

15. Delavari H., Zolfi M. Maximum power point tracking in photovoltaic systems using indirect adaptive fuzzy robust controller. *Soft Computing*, 2021, vol. 25, no. 16, pp. 10969-10985. doi: https://doi.org/10.1007/s00500-021-05823-0.
16. Yang B., Yu T., Shu H., Zhu D., An N., Sang Y., Jiang L. Perturbation observer based fractional-order sliding-mode controller for MPPT of grid-connected PV inverters: Design and real-time implementation. *Control Engineering Practice*, 2018, vol. 79, pp. 105-125. doi: https://doi.org/10.1016/j.conengprac.2018.07.007.
17. Ali A.I.M., Mohamed H.R.A. Improved P&O MPPT algorithm with efficient open-circuit voltage estimation for two-stage grid-integrated PV system under realistic solar radiation. International *Journal of Electrical Power & Energy Systems*, 2022, vol. 137, art. no. 107805. doi: https://doi.org/10.1016/j.ijepes.2021.107805.
18. Roselyn J.P., Chandran C.P., Nithya C., Devaraj D., Venkatesan R., Gopal V., Madhura S. Design and implementation of fuzzy logic based modified real-reactive power control of inverter for low voltage ride through enhancement in grid connected solar PV system. *Control Engineering Practice*, 2020, vol. 101, art. no. 104494. doi: https://doi.org/10.1016/j.conengprac.2020.104494.
19. Ahmed M., Abdelrahem M., Farhan A., Harbi I., Kennel R. DC-link sensorless control strategy for grid-connected PV systems. *Electrical Engineering*, 2021, vol. 103, no. 5, pp. 2345-2355. doi: https://doi.org/10.1007/s00202-021-01228-2.
20. López Seguel J., Seleme S.I., Moráis L.M.F. Comparison of the performance of MPPT methods applied in converters Buck and Buck-Boost for autonomous photovoltaic systems. *Ingeniare. Revista Chilena de Ingeniería*, 2021, vol. 29, no. 2, pp. 229-244. doi: https://doi.org/10.4067/S0718-33052021000200229.
21. Boumaaraf H., Talha A., Bouhali O. A three-phase NPC grid-connected inverter for photovoltaic applications using neural network MPPT. *Renewable and Sustainable Energy Reviews*, 2015, vol. 49, pp. 1171-1179. doi: https://doi.org/10.1016/j.rser.2015.04.066.
22. Hai T., Zhou J., Muranaka K. An efficient fuzzy-logic based MPPT controller for grid-connected PV systems by farmland fertility optimization algorithm. *Optik*, 2022, vol. 267, art. no. 169636. doi: https://doi.org/10.1016/j.ijleo.2022.169636.
23. Bhunia M., Subudhi B., Ray P.K. Design and Real-Time Implementation of Cascaded Model Reference Adaptive Controllers for a Three-Phase Grid-Connected PV System. *IEEE Journal of Photovoltaics*, 2021, vol. 11, no. 5, pp. 1319-1331. doi: https://doi.org/10.1109/JPHOTOV.2021.3093047.
24. Charaabi A., Zaidi A., Barambones O., Zanzouri N. Implementation of adjustable variable step based backstepping control for the PV power plant. *International Journal of Electrical Power & Energy Systems*, 2022, vol. 136, art. no. 107682. doi: https://doi.org/10.1016/j.ijepes.2021.107682.
25. Repak M., Otcenasova A., Altus J., Regula M. Grid-tie power converter for model of photovoltaic power plant. *Electrical Engineering*, 2017, vol. 99, no. 4, pp. 1377-1391. doi: https://doi.org/10.1007/s00202-017-0611-6.
26. Shayestegan M. Overview of grid-connected two-stage transformer-less inverter design. *Journal of Modern Power Systems and Clean Energy*, 2018, vol. 6, no. 4, pp. 642-655. doi: https://doi.org/10.1007/s40565-017-0367-z.
27. Ali A.I.M., Sayed M.A., Mohamed E.E.M. Modified efficient perturb and observe maximum power point tracking technique for grid-tied PV system. *International Journal of Electrical Power & Energy Systems*, 2018, vol. 99, pp. 192-202. doi: https://doi.org/10.1016/j.ijepes.2017.12.029.

Received 19.12.2022
Accepted 21.01.2023
Published 01.09.2023

Nora Zerzouri[1]*, Doctor of Technical Sciences,*
Nadia Ben Si Ali[1]*, Professor of Electrical Engineering,*
Nadia Benalia[1]*, Doctor of Technical Sciences,*
[1] Electrical Engineering Laboratory of Annaba,
Badji Mokhtar University Annaba, Algeria,
e-mail: nora.zerzouri@univ-annaba.dz (Corresponding Author);
bensialin@yahoo.fr; benalianadia13@yahoo.com

How to cite this article:
Zerzouri N., Ben Si Ali N., Benalia N. A maximum power point tracking of a photovoltaic system connected to a three-phase grid using a variable step size perturb and observe algorithm. *Electrical Engineering & Electromechanics*, 2023, no. 5, pp. 37-46. doi: https://doi.org/10.20998/2074-272X.2023.5.06